Cell Metabolism
Article

Pten Positively Regulates Brown Adipose Function, Energy Expenditure, and Longevity

Ana Ortega-Molina,[1] Alejo Efeyan,[1] Elena Lopez-Guadamillas,[1] Maribel Muñoz-Martin,[1] Gonzalo Gómez-López,[2] Marta Cañamero,[3] Francisca Mulero,[4] Joaquin Pastor,[5] Sonia Martinez,[5] Eduardo Romanos,[6] M. Mar Gonzalez-Barroso,[7] Eduardo Rial,[7] Angela M. Valverde,[8,9] James R. Bischoff,[5] and Manuel Serrano[1,*]
[1]Tumor Suppression Group
[2]Bioinformatics Unit
[3]Comparative Pathology Unit
[4]Molecular Imaging Unit
[5]Experimental Therapeutics Program
Spanish National Cancer Research Center (CNIO), Madrid E28029, Spain
[6]Phenotyping Unit, Aragon Health Sciences Institute, Zaragoza E50009, Spain
[7]Department of Cellular and Molecular Medicine, Centro de Investigaciones Biológicas (CSIC), Madrid E28040, Spain
[8]Institute of Biomedicine Alberto Sols (CSIC/UAM), Madrid E28029, Spain
[9]Centro de Investigación Biomédica en Red de Diabetes y Enfermedades Metabólicas Asociadas, ISCIII, Spain
*Correspondence: mserrano@cnio.es
DOI 10.1016/j.cmet.2012.02.001

SUMMARY

Aging in worms and flies is regulated by the PI3K/Akt/Foxo pathway. Here we extend this paradigm to mammals. *Pten*^{tg} mice carrying additional genomic copies of *Pten* are protected from cancer and present a significant extension of life span that is independent of their lower cancer incidence. Interestingly, *Pten*^{tg} mice have an increased energy expenditure and protection from metabolic pathologies. The brown adipose tissue (BAT) of *Pten*^{tg} mice is hyperactive and presents high levels of the uncoupling protein Ucp1, which we show is a target of Foxo1. Importantly, a synthetic PI3K inhibitor also increases energy expenditure and hyperactivates the BAT in mice. These effects can be recapitulated in isolated brown adipocytes and, moreover, implants of *Pten*^{tg} fibroblasts programmed with Prdm16 and Cebpβ form subcutaneous brown adipose pads more efficiently than wild-type fibroblasts. These observations uncover a role of Pten in promoting energy expenditure, thus decreasing nutrient storage and its associated damage.

INTRODUCTION

Tumor suppressors are best known for their ability to provide organisms with protection against cancer. At a deeper level, however, tumor suppressors appear to protect cells from many types of damage not necessarily related to cancer. In this regard, an emerging theme in the study of tumor suppressors is their pleiotropic beneficial effects on multiple aspects of physiology, including aging (Serrano and Blasco, 2007). Evidence for a simultaneous protection from cancer and aging exists for tumor suppressors p53, Ink4a, and Arf (Matheu et al., 2007, 2009). Here we have set to test this paradigm for the tumor suppressor Pten. Together, Pten, p53, Ink4a, and Arf constitute the four most important tumor suppressors in mammals as reflected by their overall high frequency of inactivation in a wide range of cancer types.

The most prominent function of Pten is to counteract the activity of phosphatidylinositol 3-kinase type I (PI3K) (Chalhoub and Baker, 2009). These kinases mediate signals triggered by insulin, insulin-like growth factors, and other molecules generally involved in cellular growth, metabolism, survival, and proliferation. Activation of PI3K is followed by the activation of Akt, which in turn triggers a complex cascade of events that include the inhibition of Foxo transcription factors as well as feedback loops that ensure that the activity of the pathway is kept within limits (Carracedo and Pandolfi, 2008; Kamagate et al., 2010; Matsumoto et al., 2006; Puig and Tjian, 2005; Um et al., 2006). A number of genetically modified animals with decreased activity of the insulin and Igf1 signaling (IIS) axis are characterized by an extended longevity (Fontana et al., 2010; Kenyon, 2010). In the case of the nematode *Caenorhabditis elegans*, both decreased PI3K (AGE-1) activity and increased Pten (DAF-18) expression result in extended longevity (Dorman et al., 1995; Masse et al., 2005; Morris et al., 1996). In the case of mammals, a variety of mice with decreased IIS activity have an extended longevity (Bartke, 2008). Also, caloric restriction (CR) is a robust antiaging intervention (Fontana et al., 2010), which, in mice, has been associated with decreased levels of Igf1 and reduced basal levels of PI3K pathway activity (Hempenstall et al., 2010; Jiang et al., 2008; Moore et al., 2008). However, direct inhibition of PI3K/Akt in mice has not been informative regarding longevity, because severe inhibition of these kinases results in pathological defects, diseases, and premature lethality (Renner and Carnero, 2009).

Here we have performed transgenesis with a large genomic segment carrying the intact *Pten* gene in a bacterial artificial chromosome (BAC). This has allowed us to increase the gene dosage of *Pten* and obtain a homogeneous and moderate overexpression of Pten while retaining its normal pattern of tissue

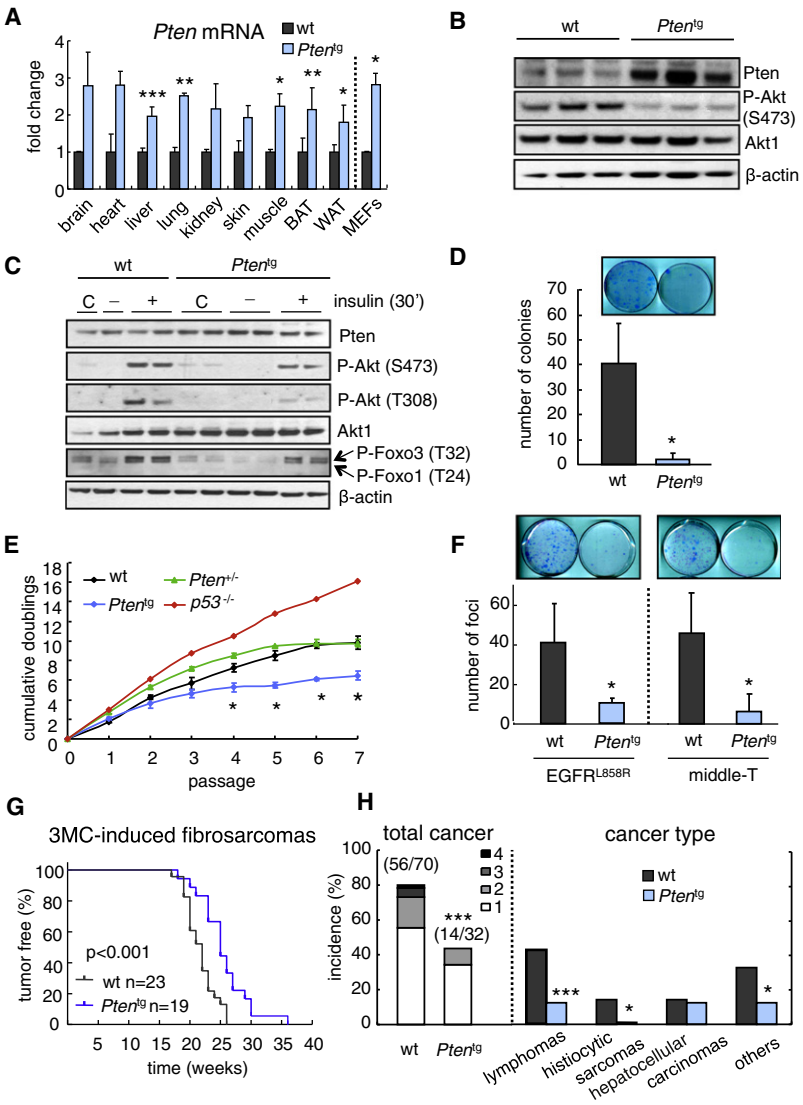

Figure 1. Characterization of *Pten*^{tg} Mice

(A) Relative *Pten* mRNA levels of the indicated tissues. Bars represent mean ± SD (n = 3 per genotype). Statistical significance was determined by the two-tailed Student's t test.

(B) Immunoblot of the indicated proteins in growing cultures of primary MEFs. Each lane corresponds to an independent MEF preparation.

(C) Lysates from normal growing (C), serum starved (–), or starved and stimulated with insulin (+) immunoblotted to detect the indicated proteins.

(D) Primary MEFs (2×10^4) were plated at very low density, and the number of colonies was scored 3 weeks after. Bars represent mean ± SD (n = 3 independent MEF preparations per genotype). Representative plates are shown in the top. Statistical significance was determined by the two-tailed Student's t test.

(E) Primary MEFs were serially cultured (according to the 3T3 protocol) and the number of accumulated population doublings is scored at each passage. Values correspond to the mean ± SD (n = 3 independent MEF preparations per genotype). Statistical significance was determined by the two-tailed Student's t test.

(F) Neoplastic foci in MEFs retrovirally transduced with the viral oncoprotein E6 and either one of the indicated PI3K-dependent oncogenes, EGFR^{L858R} or polyoma virus middle-T. Bars represent mean ± SD (n = 3 independent MEF preparations per genotype). Representative plates are shown in the top. Statistical significance was determined by the two-tailed Student's t test.

(G) Chemical carcinogenesis with 3-methyl-cholanthrene (3MC). Tumor-free Kaplan-Meier curves. Time is post-3MC injection. Statistical significance was determined by the log rank test.

(H) Incidence of cancers. Percentage of mice with one malignant tumor, or more (2–4), as indicated (left). Percentage of mice with the indicated type of tumor (right). Statistical significance was determined by the Fisher's exact test.

*p < 0.05; **p < 0.01; ***p < 0.001. See also Figure S1.

expression. An important additional benefit of BAC transgenesis is that it allows the discovery of new physiological functions that may not be uncovered using other approaches such as gene deletion or tissue-restricted overexpression. Additionally, BAC transgenesis models the effects of a systemic pharmacological intervention aimed at enhancing Pten activity. This is particularly relevant given the current development of pharmacologically active small compound PI3K inhibitors. In this work, we report the discovery of an unsuspected function of Pten in the regulation of brown adipose function, energy expenditure, and protection from metabolic damage.

RESULTS

Pten^{tg} Mice Are Protected from Cancer

To augment Pten activity without incurring overt imbalances, we performed transgenesis with a BAC carrying a large (127 kb) intact genomic segment that includes the complete murine *Pten* gene (see Figure S1A online). In this manner, we obtained a transgenic mouse line, *Pten*^{tg}, that expresses ~2-fold levels of Pten relative to their wild-type (WT) littermates across all examined tissues, including mouse embryonic fibroblasts (MEFs) (2.3 ± 0.4; Figure 1A). Transgenic mice were fertile and viable, although analysis of the segregation of the *Pten*^{tg} allele indicated that the frequency of weaned transgenic mice was lower than expected (~50% lower) (Table S1). Examination of embryos at an advanced stage of gestation (E13.5) showed equal proportions of WT and transgenic genotypes (Table S1), albeit transgenic embryos were noticeably smaller than WT embryos (Figure S1B). We surmise that the small size of the transgenic pups could cause abandonment by the mothers and early postnatal lethality. It is worth mentioning that a similarly high proportion of postnatal lethality has been reported for the long-lived dwarf mice deficient in the growth hormone receptor (*Ghr*) (Coschigano et al., 2003; Zhou et al., 1997). The functionality of the *Pten* transgene was validated genetically by its ability to rescue the tumor-prone phenotype of *Pten*$^{+/-}$ mice and the embryonic lethality of *Pten*$^{-/-}$ embryos (Di Cristofano et al., 1998; Podsypanina et al., 1999; Suzuki et al., 1998). Specifically, *Pten*$^{+/-;tg}$ mice had a longevity comparable to *Pten*$^{+/+}$ mice

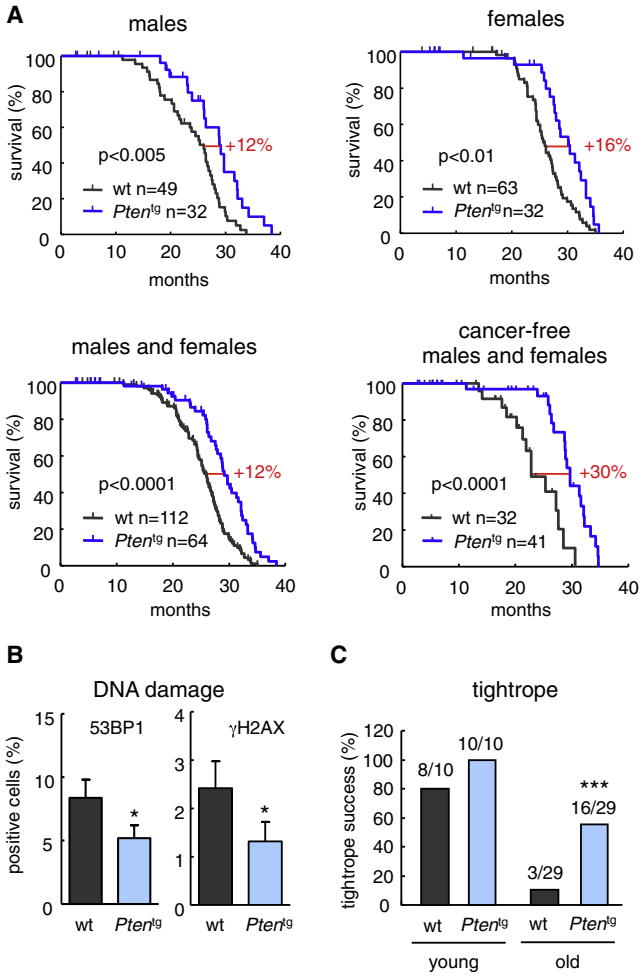

Figure 2. Increased Longevity of *Pten*^{tg} Mice

(A) Kaplan-Meier survival curves. Numbers in red indicate the relative increase in median survival. The right bottom graph corresponds to those mice that were free of detectable malignant tumors at the time of death. Statistical significance was determined by the log rank test.

(B) DNA damage in the liver of old mice (1.5–2 years old; n = 4 males per genotype). Percentage of positive nuclei by immunofluorescence using the indicated markers (mean ± SD). Statistical significance was determined by the two-tailed Student's t test.

(C) Neuromuscular coordination. Tightrope assay in young (4–6 months) and old (1.5–2 years) mice (mixed sexes) of the indicated genotypes (number of mice that passed the test versus total number of tested mice). Statistical significance was determined by the Fisher's exact test.

*p < 0.05; ***p < 0.001. See also Figure S2.

(Figure S1C), and *Pten*$^{-/-;tg}$ embryos were viable and reached adulthood (data not shown).

The impact of Pten overexpression on PI3K signaling was confirmed in primary MEFs under standard culture conditions in which the basal levels of Pten protein were clearly increased in association with lower levels of phosphorylated Akt (phospho-Ser473-Akt) (Figure 1B). Also, insulin-triggered PI3K signaling was attenuated as judged by the levels of phospho-Ser473-Akt and phospho-Thr308-Akt, as well as phospho-Thr24-Foxo1 and phospho-Thr32-Foxo3 (Figure 1C; Figure S1D). To evaluate whether the *Pten* transgene had an effect on the proliferation of MEFs, we measured their ability to form colonies at low density and to accumulate population doublings upon serial passages. In both assays, *Pten*^{tg} MEFs demonstrated a poorer proliferative capacity compared to WT MEFs (Figures 1D and 1E). Next, we asked whether the *Pten* transgene was able to protect primary MEFs from oncogenic transformation. For this, we introduced into MEFs the papilloma virus oncoprotein E6, which inactivates p53, together with either oncogenic EGFR (EGFR^{L858R}) or polyoma virus oncoprotein middle-T, whose oncogenic activities are known to be strictly dependent on PI3K signaling (Utermark et al., 2007; Zhao et al., 2006). In both cases, *Pten*^{tg} MEFs were significantly more resistant than WT MEFs to oncogenic transformation (Figure 1F). Finally, we examined whether tumor suppression, the archetypical activity of Pten, was enhanced in *Pten*^{tg} mice. This was evaluated, first, using a chemical carcinogenesis assay consisting of intramuscular injection of 3-methyl-cholanthrene (3MC). This cancer model generates fibrosarcomas in all the treated mice, but *Pten*^{tg} mice showed a significantly extended tumor-free survival compared to WT mice (Figure 1G). Additionally, we performed complete histological exploration of aged moribund mice and scored the incidence of tumors (nonmalignant and malignant), as well as other pathologies (Table S2). Interestingly, the percentage of old moribund mice with cancer (i.e., malignant tumors) was significantly reduced in the *Pten*^{tg} group relative to WT mice (Figure 1H). Several cancer types, most notably lymphomas and histiocytic sarcomas, were significantly reduced in the *Pten*^{tg} cohort (Figure 1H). These observations are in concordance with the fact that *Pten* haploinsufficiency produces a variety of tumor types, most notably including lymphomas (Di Cristofano et al., 1998; Podsypanina et al., 1999; Stambolic et al., 2000). We conclude that the *Pten*^{tg} allele is functional and provides protection against neoplastic transformation and cancer.

Pten^{tg} Mice Live Longer

To address the impact of Pten on health span and longevity, we followed cohorts of *Pten*^{tg} mice, together with their WT littermates, during their entire life span (Tables S3 and S4). Importantly, both male and female *Pten*^{tg} mice showed a significant increase in longevity as indicated by their Kaplan-Meier survival curves, median survival, and maximal life span (Figure 2A; Tables S5 and S6; Figures S2A and S2B). In particular, the mean longevity of the oldest 20% mice was significantly increased both in males (+16%) and in females (+9%) (p values of 0.003 and 0.009, respectively), and the mean longevity of the oldest 10% of mice was also significantly increased in both sexes (Table S6). Additional statistical tests (Cox regression) indicated that the increased survival of *Pten*^{tg} mice was dependent on the transgene and independent of other variables, such as the identity of the parents or the date of birth (Table S7). We also wondered whether the effect of the transgene in longevity was a consequence of its protective effect on cancer. However, cancer-free *Pten*^{tg} mice also showed an increased longevity when compared with cancer-free WT mice (Figure 2A). This indicates that *Pten*^{tg} extends longevity independently of its effect on cancer protection and suggests a direct impact on health span. The accumulation of DNA damage within tissues, and particularly in the liver, is a robust biomarker of aging (Matheu et al.,

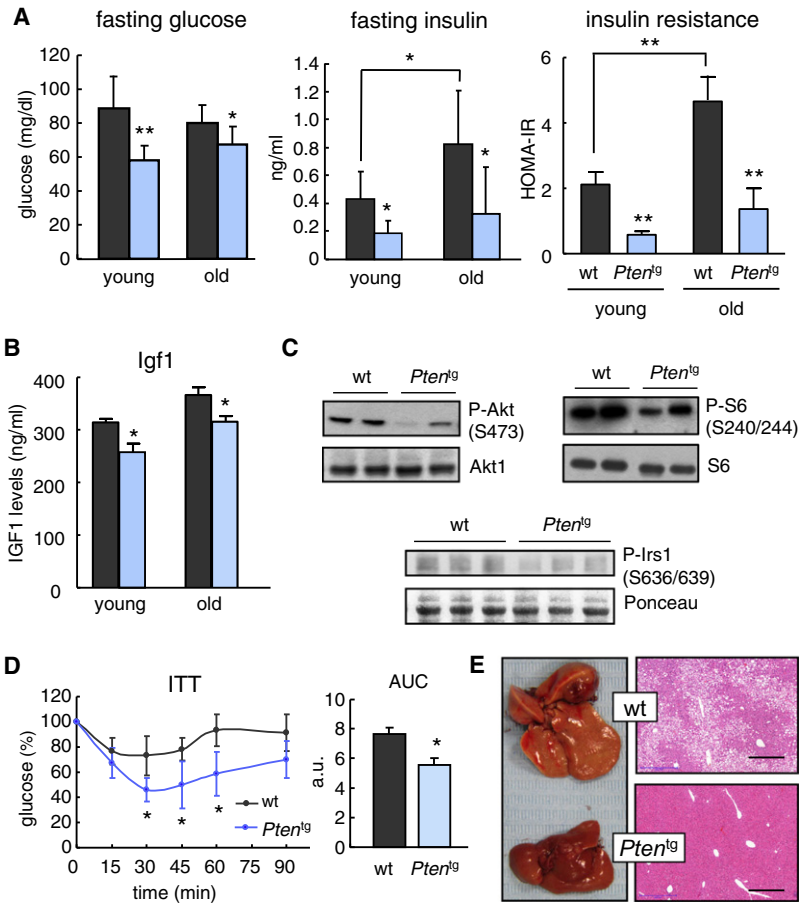

Figure 3. Improved Insulin Sensitivity and Protection from Diet-Induced Steatosis in *Pten*^{tg} Mice

(A) Fasting glucose and insulin, and its derived insulin resistance index HOMA-IR (n = 5–7 males per genotype and per age group). Young, 4–6 months old; old, 1.5–2 years old.

(B) Igf1 levels in serum (n = 4 males per genotype and per age group). Age groups as in (A).

(C) Immunoblot of the indicated proteins from epididymal WAT. Each lane corresponds to a different mouse. Irs1 corresponds to old male mice (1.5–2 years old).

(D) Insulin sensitivity of mice chronically fed with HFD for 6 months. Insulin sensitivity was measured by ITT. The graph to the right quantifies the area under the curve (AUC).

(E) Macroscopic views of representative livers 6 months after chronic HFD and microscopic sections stained with hematoxylin and eosin (bar indicates 500 μm).

All values correspond to mean ± SD, and statistical significance was determined by the two-tailed Student's t test. *p < 0.05; **p < 0.01. See also Figure S3.

2007; Wang et al., 2009). Immunofluorescence with two markers of DNA damage, 53BP1 and γH2AX, indicated a significantly lower level of DNA damage in the liver of old *Pten*^{tg} mice compared to WT controls (Figure 2B). Also, old transgenic mice (1.5–2 years old) performed better in the tightrope test than WT controls (Figure 2C), further suggesting improved health span, although interpretation of this test could be confounded by the different weight of the mice (see below). We conclude that moderate overexpression of *Pten* improves markers of healthy aging and increases longevity independently of cancer protection.

Pten^{tg} Mice Are Protected from Insulin Resistance and Steatosis

A widespread feature of long-lived mice with decreased IIS axis activity is their improved insulin sensitivity (Bartke, 2008). This effect, apparently paradoxical, is explained by the concomitant reduction in the negative feedback routes that emanate from the insulin signaling pathway (Carracedo and Pandolfi, 2008; Kamagate et al., 2010; Matsumoto et al., 2006; Puig and Tjian, 2005). In keeping with this, *Pten*^{tg} mice, both young (4–6 months old) and old (1.5–2 years old), had lower fasting levels of glucose and insulin serum levels (Figure 3A), and a significantly lower value of the insulin resistance index HOMA-IR (Figure 3A) (see also QUICKI index in Figure S3A). Also, serum levels of Igf1 were significantly, albeit moderately, lower in *Pten*^{tg} mice compared to WT mice, at both young and old ages (Figure 3B). To explore the role of negative feedback signals in white adipose tissue (WAT), we examined the levels of S6K activity, which is a main activity responsible for negative feedback signaling (Um et al., 2004, 2006). As expected, the WAT of *Pten*^{tg} mice presented reduced levels of phosphorylated Akt and, interestingly, lower levels of phosphorylation in two relevant substrates of S6K, namely S6 and Irs1 (Figure 3C). S6K-mediated phosphorylation of Irs1 at Ser636/639 is inhibitory for insulin signaling and, analogously to the phenotype of S6K1 null mice (Um et al., 2004), the lower activity of S6K in *Pten*^{tg} mice could explain their improved insulin sensitivity. To further challenge this concept, we fed mice with high-fat diet (HFD) for 6 months, which is a well-established metabolic stress that produces insulin resistance and liver steatosis. Under HFD, *Pten*^{tg} mice increased their body weight to a relative extent similar to that of WT mice (Figure S3B). However, upon injection of insulin (insulin tolerance test, ITT), HFD-fed WT mice were unresponsive to insulin, while HFD-fed *Pten*^{tg} mice responded to insulin with a significant decrease in glucose levels (Figure 3D). Moreover, HFD-fed WT mice had overt liver steatosis, while HFD-fed *Pten*^{tg} mice had minimal or no signs of steatosis (Figure 3E). All together, we conclude that moderate and regulated overexpression of Pten results in improved insulin sensitivity and in protection from the damaging effects of HFDs.

Increased Energy Expenditure in *Pten*^{tg} Mice

In an effort to shed light onto the physiological mechanisms involved in the extended life span of *Pten*^{tg} mice and their protection against damage induced by nutrient overload, we have explored their metabolism. *Pten*^{tg} mice presented a decreased body weight (Figure 4A) (27% and 28% decrease in young [4–6 months old] male and female mice, respectively, and 35% and 44% in old [1–2 years old] males and females; Figure S4A).

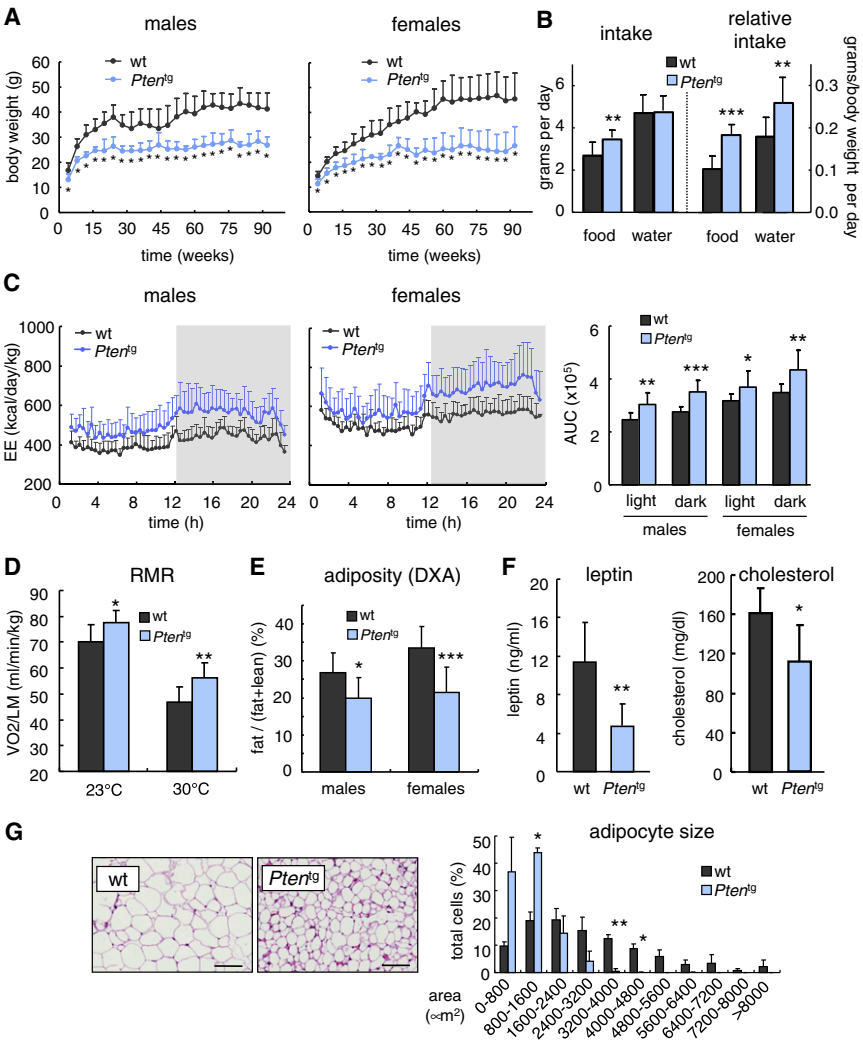

Figure 4. Elevated Energy Expenditure and Decreased Adiposity in *Pten*^{tg} Mice

(A) Weight curves (n = 15 for each genotype and sex).

(B) Food intake in absolute values (left) and normalized by body weight (right) (n = 8 males per genotype; 3–4 months old).

(C) Energy expenditure measured in adult males and females (6–8 months old; n = 8–10 per genotype and per sex). The bar graph at the right side represents the AUC over the indicated 12 hr period.

(D) Resting metabolic rate measured at the indicated temperatures in adult males (6–8 months old; n = 7–9 per genotype).

(E) Adiposity in young mice (6–8 months old; n = 8–10 per genotype and per sex) measured by dual energy X-ray absorptiometry (DXA). Values correspond to the percentage of fat relative to the sum of lean and fat masses.

(F) Leptin and cholesterol levels in the serum of young mice (n = 8 males per genotype; 6 months old).

(G) Representative picture of epididymal WAT. Samples correspond to young males and were stained with hematoxylin and eosin (bar indicates 100 mm) (left). Adipocyte area distribution is shown (n = 2 per genotype; >500 cells per genotype) (right).

All values correspond to mean ± SD, and statistical significance was determined by the two-tailed Student's t test. *p < 0.05; **p < 0.01; ***p < 0.001. See also Figure S4.

Interestingly, this lower weight occurred despite the fact that *Pten*^{tg} mice were hyperphagic (Figure 4B and Figure S4B). We wondered whether this could be a result of increased energy expenditure. Indirect calorimetry indicated that *Pten*^{tg} mice have an increased energy expenditure relative to their total body weight and under normal housing conditions (23°C and access to water and food) (Figure 4C). Following recent recommendations on how to compare energy expenditure between groups with different body weights (Arch et al., 2006; Kaiyala and Schwartz, 2011), we applied more stringent statistical tests (general linear model [GLM] and analysis of covariance [ANCOVA]). However, applying these tests we could not detect a significant impact of the transgene on energy expenditure under these conditions. To improve the sensitivity of the calorimetric measurements, we scored the resting metabolic rate (RMR) at 23°C and, more importantly, at 30°C (thermoneutrality) in the absence of water and food. This minimizes the contributions of physical activity, food processing, and body temperature maintenance on energy expenditure, thus allowing a more accurate evaluation of the differences in basal metabolism. Moreover, due to the different body composition of the *Pten*^{tg} mice (see below), we followed recent recommendations regarding the use of lean mass rather than total body weight for normalization (Butler and Kozak, 2010). Importantly, *Pten*^{tg} mice had an increased RMR relative to lean mass, both at 23°C and 30°C (Figure 4D). Furthermore, in this case, GLM and ANCOVA analyses indicated that the transgene has a statistically significant impact on metabolic rate, which is independent of its effect on lean mass (Figure S4C). No significant changes were detected in the respiratory quotient (Figure S4D). Locomotor activity and body temperature were similar between the two cohorts of mice (Figures S4E and S4F), thus excluding these factors as possible explanations for the increased energy expenditure, and implying an elevated metabolic rate as responsible for the observed increase in energy expenditure.

High levels of energy expenditure are generally associated with reduced nutrient storage and protection from metabolic damage. In support of this, dual energy X-ray absorptiometry (DXA) indicated that *Pten*^{tg} mice had a relative decrease in fat mass (Figure 4E; Figure S4G). Also, compared to WT controls, the weight of the epididymal WAT relative to body weight was significantly lower in transgenic males (Figure S4H), and their serum levels of leptin and cholesterol were reduced compared to WT mice (Figure 4F). Finally, the size of the adipocytes in the epididymal WAT was smaller (Figure 4G). Incidentally, adiponectin and thyroxine levels were normal in *Pten*^{tg} mice

(Figure S4I). Together, these results indicate that moderate upregulation of Pten results in increased energy expenditure and lower adiposity.

Pten^{tg} Mice Have a Hyperactive BAT

An efficient mechanism to dissipate energy is through brown adipocytes, which are located both at the brown adipose tissue (BAT) and also interspersed within the WAT (Kozak and Anunciado-Koza, 2008; Nedergaard and Cannon, 2010). Brown adipocytes have gained considerable attention since the recent recognition of their relevance in adult humans (Cypess et al., 2009; Lidell and Enerback, 2010; van Marken Lichtenbelt et al., 2009; Virtanen et al., 2009). Moreover, in mice, the magnitude of nutrient uptake by the BAT is comparable to that of the liver under normal temperature and diet conditions (Bartelt et al., 2011; Nedergaard et al., 2011). Macroscopically, the interscapular BAT of *Pten*^{tg} mice had a more intense color compared to WT BAT and, histologically, it presented a denser appearance due to reduced size of the multilocular lipid droplets (Figure 5A), which is suggestive of higher BAT activity. To directly assess the constitutive activity of the BAT, we measured ^{18}F-deoxyglucose (FDG) uptake by positron emission tomography (PET). Importantly, the uptake of glucose was significantly higher in the BAT of *Pten*^{tg} mice compared to the BAT of WT mice (Figure 5B). Energy dissipation in brown adipocytes is mediated by the uncoupling protein Ucp1 (Nicholls and Locke, 1984). Remarkably, the expression levels of *Ucp1* were significantly higher in the BAT of *Pten*^{tg} mice compared to their WT littermates (Figure 5C). In relation to this, it is worth mentioning that mice lacking the insulin receptor (IR) in the BAT also present higher levels of *Ucp1* expression (Guerra et al., 2001).

The transcriptional coactivator Pgc1α is a critical positive regulator of *Ucp1* expression and regulates multiple metabolic responses including the induction of fatty acid oxidation (Puigserver and Spiegelman, 2003; Puigserver et al., 1998; Vega et al., 2000). Interestingly, *Pgc1a* and some genes involved in fatty acid oxidation were also significantly upregulated in the BAT of *Pten*^{tg} mice (Figure 5C). Other genes expressed in brown adipocytes were not significantly altered (Figure S5A). In the liver, the transcriptional factor Foxo1 is an essential partner for the function of Pgc1α (Matsumoto et al., 2007; Puigserver et al., 2003), and Akt phosphorylates and inhibits both Pgc1α (Li et al., 2007) and Foxo proteins (Kops et al., 1999; van der Horst and Burgering, 2007). Based on this, we examined whether the BAT of *Pten*^{tg} mice also had lower levels of phosphorylated Akt and Foxo1. Indeed, immunodetection of these proteins revealed that transgenic BAT had lower levels of active Akt (phospho-Ser473-Akt) as well as lower levels of phosphorylated Foxo1 (phospho-Thr24-Foxo1) (Figure 5D). Incidentally, we wondered whether CR would exert a similar transcriptional response in the BAT, but mice under CR for 4 weeks presented lower, rather than higher, levels of *Pgc1a* and normal levels of *Ucp1* in the BAT (Figure S5B).

Both *Pgc1a* and *Ucp1* are characteristically expressed in brown, but not in white, adipocytes (Puigserver and Spiegelman, 2003; Puigserver et al., 1998), and therefore their detection in WAT is indicative of the presence of brown adipocytes within WAT (Kozak and Anunciado-Koza, 2008; Nedergaard and Cannon, 2010). Analysis of subcutaneous WAT (inguinal, iWAT) showed significantly higher levels of *Pgc1a* and *Ucp1* expression in transgenic mice compared to WT mice (Figure 5E), and histological analyses and Ucp1 immunohistochemistry detected the presence of abundant brown adipocytes interspearsed within white adipocytes (Figure 5F). Increased levels of *Pgc1a* and *Ucp1* were also found in visceral WAT (epididymal, eWAT) (Figure S5C). Together these observations indicate widespread presence of brown adipocytes within the WAT of *Pten*^{tg} mice. In addition to brown adipocytes, muscle is another important tissue responsible for energy expenditure. In particular, overexpression of Pgc1α or small compounds that activate Pgc1α through Sirt1 induce a change in muscle myofibers from type II (low oxidative capacity) to type I (high oxidative capacity), and this is associated with increased energy expenditure (Feige et al., 2008; Lin et al., 2002). Examination of succinate dehydrogenase in the gastrocnemius muscle (containing both types of myofibers), as well as the expression levels of genes characteristic of type I and type II myofibers, oxidative phosphorylation genes, and mitochondrial DNA, did not reveal differences between WT and *Pten*^{tg} mice (Figure S5D). This reinforces the idea that the increased energy expenditure observed in *Pten*^{tg} mice is at least partially due to a higher activity of brown adipocytes.

The above observations demonstrating an increased activity of brown adipocytes in *Pten*^{tg} mice could be due, at least to some extent, to the small body size of these mice, which implies higher rates of body heat loss. To study the intrinsic effect of PI3K inhibition on brown adipocyte function, we undertook two approaches: to analyze the role of the PI3K pathway on isolated cells, and to examine the effect of pharmacological inhibition of PI3K in WT mice (see further below). To study the regulation of brown adipocyte function in vitro, we established immortalized cultures of neonatal brown adipocytes (undifferentiated pre-brown adipocytes) from WT and *Pten*^{tg} mice. Compared to WT pre-brown adipocytes, *Pten*^{tg} pre-brown adipocytes presented significantly higher levels of *Pten*, *Pgc1a*, and *Ucp1* mRNA and lower levels of phosphorylated Akt and Foxo1 (Figure 5G). To directly evaluate the thermogenic activity of pre-brown adipocytes, we measured the rate of respiration (oxygen consumption rate, OCR) in the absence or presence of oligomycin (Dranka et al., 2011). Interestingly, the proton leakage rate (respiration in the presence of oligomycin) was significantly higher in *Pten*^{tg} pre-brown adipocytes than in their WT counterparts (Figure 5H). To further support the cell-autonomous impact of Pten in pre-brown adipocytes, we reduced the levels of Pten in WT pre-brown adipocytes using shRNAs against Pten. As hypothesized, this resulted in lower levels of *Pgc1a* and *Ucp1* (Figure S5E). Finally, to directly test the implication of Foxo1, retroviral expression of constitutively active Foxo1, Foxo1-AAA (Nakamura et al., 2000), induced both *Pgc1a* and *Ucp1*, as well as *Sod2*, a known transcriptional target of Foxo1 (Figure S5F). Taken together, these results demonstrate that Pten is a positive regulator of brown adipocyte function, and this can at least partially explain the increased energy expenditure of *Pten*^{tg} mice.

Pten Improves the Reprogramming of Fibroblasts into BAT

The above results indicate that Pten has cell-autonomous effects that can be recapitulated in vitro with cultured brown adipocytes.

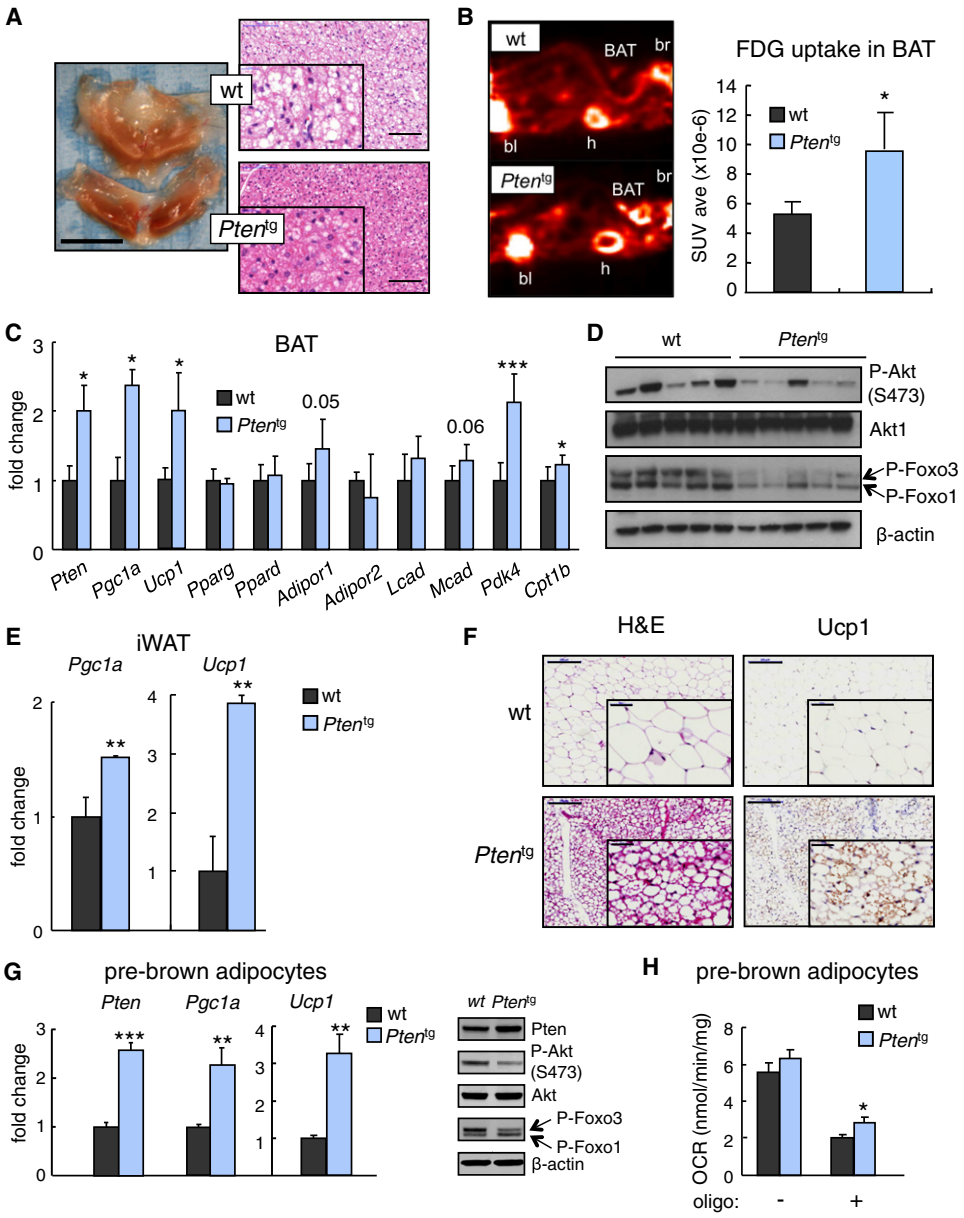

Figure 5. Hyperactive BAT in *Pten*^{tg} Mice

(A) Representative macroscopic pictures of BAT (left, bar indicates 1 cm). Microscopic pictures of BAT stained with hematoxylin and eosin (right, bars indicate 100 μm). Samples correspond to males (5 months old).

(B) ^{18}F-fluor-deoxyglucose (FDG) uptake measured by PET. Representative pictures (left). Relevant organs are indicated in addition to BAT: bl, bladder; h, heart; br, brain. Analyses were done in males (6 months old; n = 5 per genotype). Quantification of the average FDG uptake activity (standard uptake value average, SUVave) of the BAT (right).

(C) Relative gene expression in BAT (5 months old; n = 3–6 males per genotype).

(D) Immunoblot of BAT lysates (5 months old; n = 5 males per genotype).

(E) Relative gene expression in inguinal WAT (3–6 months old; n = 3 males per genotype).

(F) Representative histology and Ucp1 immunohistochemistry of the inguinal WAT from the mice in (E). Bars indicate 200 μm in high magnification pictures and 50 μm in low magnification pictures.

(G) Relative gene expression (left) and protein levels (right) in pre-brown adipoctyes (performed in triplicate cultures).

(H) Respiration rate in the absence or presence of oligomycin (oligo) in pre-brown adipocytes (values correspond to the mean ± SEM of six independent assays). Values in all panels, except (H), correspond to mean ± SD. Statistical significance was determined by the two-tailed Student's t test. *p < 0.05; **p < 0.01; ***p < 0.001. See also Figure S5.

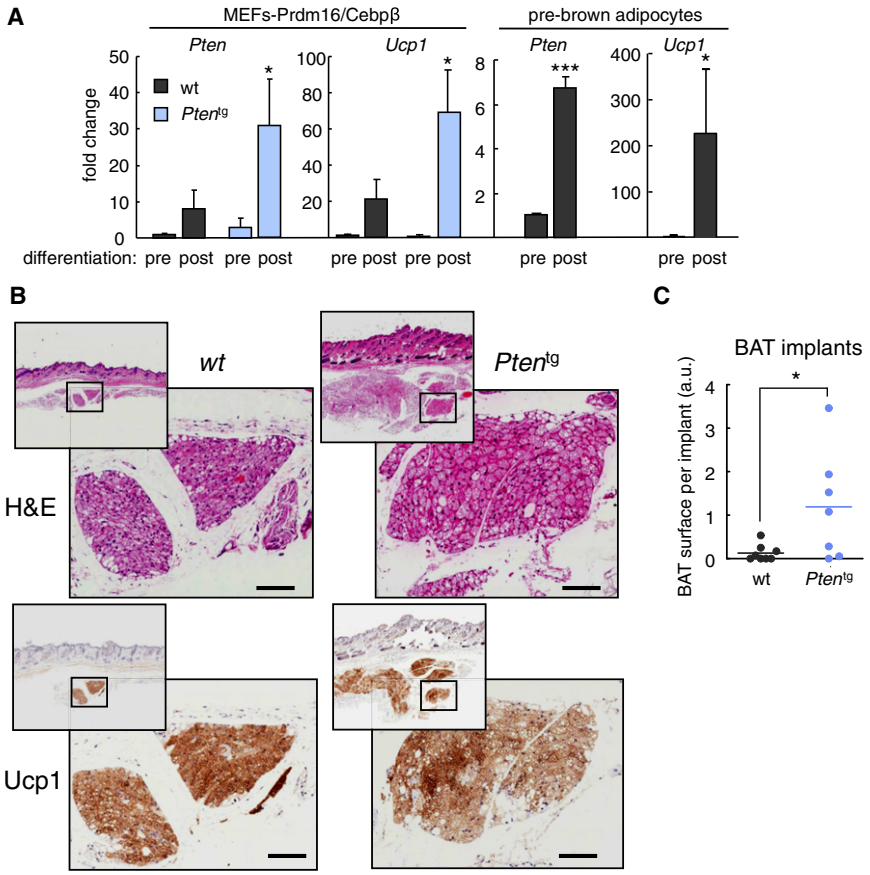

Figure 6. Reprogramming of *Pten*^{tg} MEFs into BAT

(A) Gene expression in MEFs programmed with Prdm16/Cebpβ before differentiation (pre) and after differentiation (post) into brown adipoctyes. Values correspond to the mean ± SD (n = 3) and are relative to predifferentiation WT MEFs. For comparison, pre-brown adipocytes were also differentiated in parallel.

(B) Representative microscopic pictures of BAT implants derived from Prdm16/Cebpβ-programmed WT or *Pten*^{tg} fibroblasts. Sections were stained with hematoxylin and eosin (H&E) or with anti-Ucp1 (Ucp1). Bars correspond to 200 μm. Additional pictures are shown in Figure S6.

(C) Amount of BAT formation by Prdm16/Cebpβ-programmed WT or *Pten*^{tg} fibroblasts. Each value corresponds to the area of BAT (in arbitrary units) measured in the fat pads formed per injection site (n = 8 for WT, and n = 7 for *Pten*^{tg}). Statistical significance was determined by the two-tailed Student's t test. *p < 0.05; ***p < 0.001. See also Figure S6.

To further extend this concept, we took advantage of the transcriptional factor Prdm16 and its cofactor Cebpβ, whose combined expression is able to program fibroblasts to become brown adipocytes upon in vitro differentiation and to form BAT-containing fat pads upon subcutaneous implantation (Kajimura et al., 2009; Seale et al., 2007). Immortalized WT and *Pten*^{tg} MEFs were programmed with retroviruses encoding Prdm16 and Cebpβ. Interestingly, upon in vitro differentiation into brown adipocytes, Prdm16/Cebpβ-programmed MEFs showed an upregulation of *Pten* mRNA levels, which was also observed when pre-brown adipocytes were differentiated (Figure 6A and Figure S6A). This suggests that Pten may play an active role during brown adipocyte differentiation. To directly test this in a more physiological context, Prdm16/Cebpβ-programmed MEFs were injected subcutaneously into nude mice. Two months later, fat pads with depots of BAT were identified at the injection sites (Figure 6B and Figure S6B). Quantification of the amount of BAT indicated that *Pten*^{tg} cells were significantly more efficient at generating BAT than their WT counterparts (Figure 6C). These results confirm that Pten exerts a cell-autonomous effect on BAT even in the in vivo context of a nontransgenic host (i.e., the nude mice used as host), and open a route to improve the generation of BAT implants.

Activation of BAT by PI3K Inhibitors

The mechanisms of action of Pten could go beyond the inhibition of PI3K (Song et al., 2011). To establish the involvement of PI3K on the above reported effects of Pten in BAT, we inhibited PI3K using a small compound inhibitor of PI3K developed at the Spanish National Cancer Research Center (CNIO), named CNIO-PI3Ki (see the Experimental Procedures and Figure S7A). First, we tested the effects of CNIO-PI3Ki in a total of three different models of brown adipocytes and in the absence or presence of forskolin, an activator of AMP cyclase that mimics β-adrenergic stimulation and upregulates *Ucp1* levels (Puigserver et al., 1998). Specifically, we used pre-white adipocytes 3T3-L1 ectopically expressing Cebpβ and then differentiated into brown adipocytes (Karamanlidis et al., 2007) (Figure S7B), which can be considered a model of white-to-brown transdifferentiation; we also used immortalized neonatal pre-brown adipocytes under proliferative conditions and after in vitro differentiation. Treatment of these cellular models of brown adipocytes with CNIO-PI3Ki resulted in a severe decrease in the levels of phospho-Akt (Figure 7A) and upregulation of *Pgc1a* and *Ucp1*, both alone and in combination with forskolin (Figure 7B). Moreover, treatment of pre-brown adipocytes with two other structurally unrelated inhibitors, namely GDC-0941 and LY-294002, also produced efficient induction of *Pgc1a* and *Ucp1* (Figure S7C). These results indicate that inhibition of PI3K with small compounds activates brown adipocyte function in a cell-autonomous manner. To gain additional mechanistic insight into how CNIO-PI3Ki activates the expression of *Pgc1a* and *Ucp1*, we tested binding of Foxo1 to the promoters of these genes by chromatin immunoprecipitation in differentiated brown adipocytes and in 3T3-L1/Cebpβ cells. Importantly, CNIO-PI3Ki, but not forskolin, induced the binding of Foxo1 to the promoter regions of *Pgc1a* and *Ucp1* (Figure 7C and Figure S7D). To examine the effect of CNIO-PI3Ki on brown adipocyte function, we measured the rate of proton leakage both in the

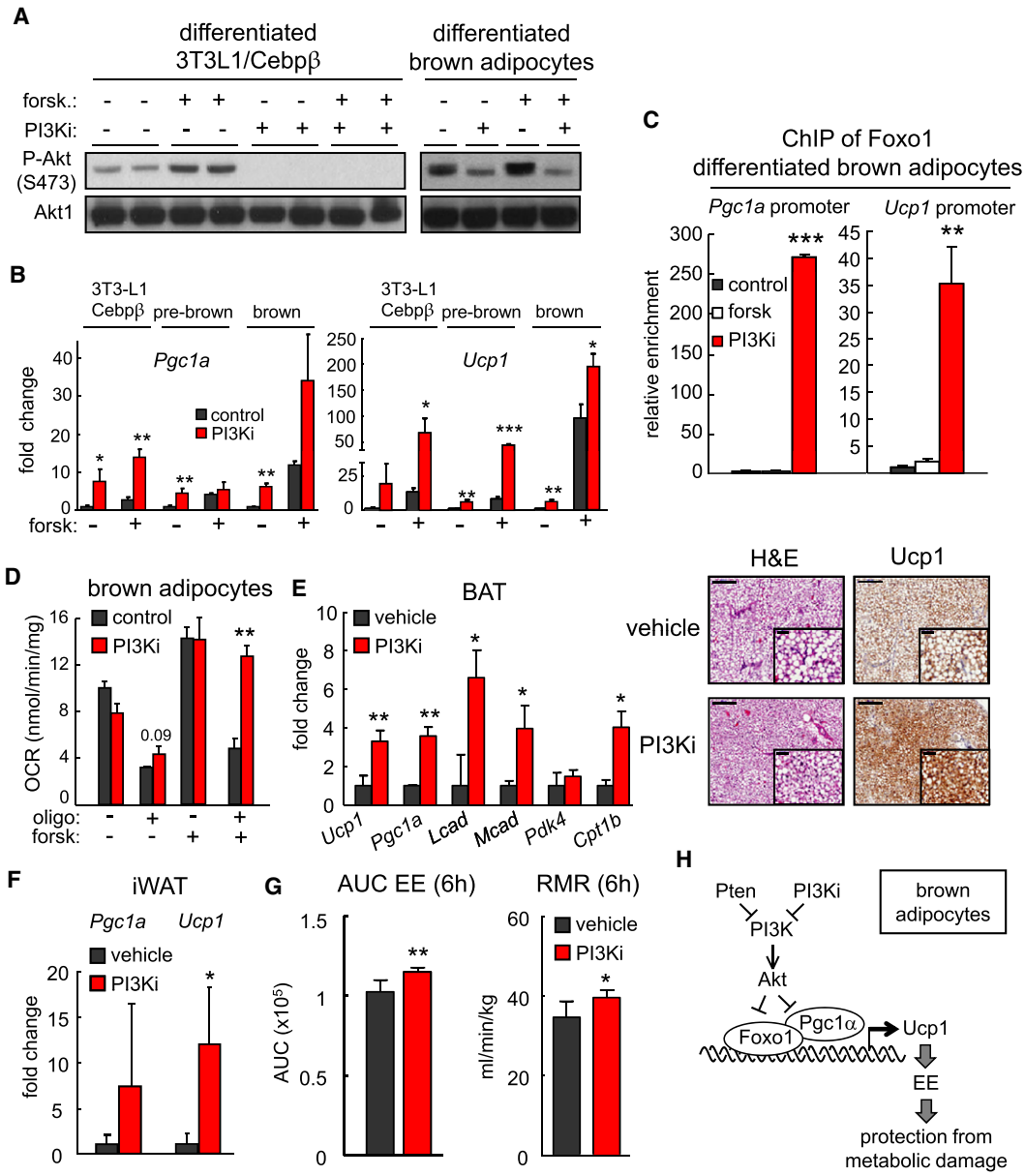

Figure 7. Recapitulation of the Effects of Pten on BAT with a PI3K Inhibitor

(A) Immunoblot of the indicated cells treated with CNIO-PI3Ki in the presence or absence of forskolin. For (A) and (B), cells were treated with forskolin (10 μM) and/or the CNIO-PI3Ki (1 μM for 3T3-L1/Cebpβ cells and pre-brown adipocytes, and 10 μM for differentiated brown adipocytes) and analyzed 4 hr later.

(B) Relative mRNA levels in the indicated cells (n = 3 independent biological repeats).

(C) ChIP of Foxo1 and PCR amplification of the *Ucp1* and *Pgc1a* promoters in differentiated brown adipocytes. Data correspond to a triplicate PCR. Similar data were obtained in a total of two assays.

(D) Respiration rate in the absence or presence of oligomycin (oligo) in differentiated brown adipocytes treated or not with CNIO-PI3Ki (10 μM) for 4 hr before measurement (values correspond to the mean ± SEM of four independent assays).

(E) Relative mRNA levels in BAT upon CNIO-PI3Ki (15 mg per kg of body weight) or vehicle administration, by gavage (3 months old; n = 3 males C57BL6 per group) (left). Samples were analyzed 6 hr after administration. Pictures correspond to representative images of the BAT stained with H&E or with anti-Ucp1 (Ucp1) (bars indicate 200 μm in high-magnification pictures and 50 μm in low-magnification pictures) (right).

(F) Relative mRNA levels in inguinal WAT (3 months old; n = 3 males per genotype).

(G) Energy expenditure (area under the curve) and resting metabolic rate were measured at 30°C in mice (3 months old; n = 5 males) treated with vehicle or CNIO-PI3Ki (15 mg/kg). Recordings from 1 to 7 hr posttreatment (a total of 6 hr) were analyzed.

(H) Summary of the effects of PI3K downregulation, by Pten or PI3Ki, on Ucp1 in brown adipocytes.

Values in all panels, except (D), correspond to mean ± SD. Statistical significance was determined by the two-tailed Student's t test. *p < 0.05; **p < 0.01; ***p < 0.001. See also Figure S7.

absence or presence of forskolin. Importantly, CNIO-PI3Ki strongly enhanced the proton leak (rate of respiration in the presence of oligomycin) of forskolin-activated brown adipocytes, while its effects were modest in the absence of activation by forskolin (Figure 7D). To further validate our data with CNIO-PI3Ki, mice were treated with this compound, and this resulted in significant upregulation of *Ucp1* and *Pgc1a*, together with some other genes involved in fatty acid oxidation in the BAT (Figure 7E), while the expression of other genes remained unaltered (Figure S7E). In addition, histology showed a decrease in the amount of lipid droplets and a more intense immunohistochemical staining of Ucp1 in the BAT of CNIO-PI3Ki-treated mice (Figure 7E). Moreover, the inguinal WAT of the treated mice also showed increased levels of *Ucp1* mRNA (Figure 7F). Finally, we wanted to test whether these effects had a reflection in energy expenditure (EE), RMR, and oxygen consumption (VO_2), all measured at 30°C and in the absence of food and water. Importantly, CNIO-PI3Ki-treated mice showed an increase in EE, RMR, and VO_2 during the analyzed period of 6 hr (from +1 hr to +7 hr postadministration) (Figure 7G and Figure S7F). Together, these results indicate that downregulation of PI3K can account for the hyperactive BAT and increased energy expenditure of *Pten*^{tg} mice. Moreover, we also conclude that the effects of PI3K inhibition on brown adipocyte activity are cell autonomous.

DISCUSSION

In worms and flies, the IIS longevity pathway is intracellularly mediated by the PI3K/Akt/Foxo pathway, where the most accepted view is that Foxo proteins orchestrate an array of protective responses, including antioxidant defenses (Fontana et al., 2010). In mammals, however, the picture is much less complete. Mice with defects in the receptors or Irs adaptors for insulin and Igf1 present increased longevity (Selman and Withers, 2011). Our findings that *Pten* transgenic mice have an increased life span contribute to extend the evolutionary conservation of this longevity pathway to mammals. However, the underlying mechanisms remain poorly understood despite intense investigation (Bartke, 2008; Fontana et al., 2010; Selman and Withers, 2011). *Pten*^{tg} mice present a number of phenotypes that have been associated to longevity in other long-lived mouse models. These phenotypes include reduced body size (Chen et al., 2010; Miller et al., 2002), reduced levels of Igf1 and improved insulin sensitivity (Bartke, 2008; Chen et al., 2010), and increased energy expenditure (Mookerjee et al., 2011). All these phenotypes could conceivably underlie the increased longevity of *Pten*^{tg} mice.

Given the lack of precedents linking Pten to energy expenditure, we have characterized this phenotype in further depth. Using rigorous calorimetric tests, we demonstrate that transgenic *Pten* mice have an increased energy expenditure, which is associated with lower adiposity and lower body weight despite being hyperphagic. Energy expenditure is a leading concept in metabolism that is emerging as a relevant determinant of longevity. Notably, a positive association has been reported between the individual values of energy expenditure of young mice and their subsequent life span (Speakman et al., 2004). The impact of energy expenditure on physiology and longevity is multifaceted. Energy expenditure associated to mitochondrial uncoupling protects cells from mitochondrial damage according to the so-called "uncoupling to survive" hypothesis (Brand, 2000; Mookerjee et al., 2011). Even if restricted to a specific tissue, increased energy expenditure has important systemic beneficial effects by consumption of nutrients, which are thereby diverted from storage and its associated systemic damage. For example, relevant for our work, localized overexpression of Ucp1 in muscle improves insulin sensitivity, protects mice under HFD from obesity and insulin resistance, and increases longevity (Gates et al., 2007; Li et al., 2000). Also, lifelong treatment of mice with a mitochondrial uncoupler increases energy expenditure and extends longevity (Caldeira da Silva et al., 2008). Consistent with their increased energy expenditure, *Pten*^{tg} mice present a number of systemic beneficial effects on health, including improved insulin sensitivity, protection from HFD-induced diabetes and steatosis, and protection from DNA damage associated to aging in the liver, which together are likely to contribute to the extended longevity of these mice.

The BAT is the paramount tissue specialized in energy dissipation through mitochondrial uncoupling. In mice under standard conditions of temperature and diet, the BAT is responsible for an amount of nutrient combustion that is similar in magnitude to the liver or the brain (Bartelt et al., 2011; Nedergaard et al., 2011). The potential relevance of the BAT to combat human obesity is based on highly suggestive correlative studies (Cypess et al., 2009; Lidell and Enerback, 2010; van Marken Lichtenbelt et al., 2009; Virtanen et al., 2009). We show with a variety of assays, including histology, functional glucose uptake, and gene expression, that the BAT of *Pten*^{tg} mice is hyperactive. This has been confirmed in in vitro assays using isolated brown adipocytes, thus indicating that the effects of Pten on brown adipocytes are, at least in part, cell autonomous. Molecular analyses, including the use of several small compound inhibitors of PI3K, have allowed us to demonstrate that the effects of Pten on brown adipocytes are mediated by the PI3K/Akt/Foxo signaling pathway that results in the activation of Ucp1 and its transcriptional regulator Pgc1α (Figure 7H). Importantly, the small compound CNIO-PI3Ki can recapitulate in vivo the upregulation of Ucp1 and Pgc1α in the BAT, and results in increased energy expenditure. Moreover, the role of Pten on brown adipocyte function has been reinforced by its ability to improve the generation of subcutaneous BAT implants from Prdm16/Cebpβ-programmed fibroblasts. Despite these evidences, we cannot exclude that Pten or pharmacological inhibition of PI3K could stimulate energy expenditure through other mechanisms in addition to the activation of brown adipocytes.

In summary, we propose that Pten is a positive regulator of energy expenditure, with a dramatic and cell-autonomous effect in the BAT. A consequence of the increased energy expenditure is a systemic protection against metabolic damage, including aging-associated insulin resistance and aging-associated DNA damage in the liver. An interesting corollary of our work is the possibility of mimicking the effects of Pten overexpression with a small compound PI3K inhibitor. In a wider scope and together with our previous reports (Matheu et al., 2007, 2009), the four main tumor suppressors, namely p53, Ink4a, Arf, and Pten, improve organismal survival independently of their effects on cancer. This reinforces the concept that these important tumor

suppressors are nodal proteins whose functions go beyond cancer and have multiple protective functions.

EXPERIMENTAL PROCEDURES

Transgenesis

Transgenesis was performed using a BAC, RP24-372O16 (obtained from CHORI; http://www.chori.org/) (Figure S1A) and following previously described procedures (Pfluger et al., 2008). Unless otherwise specified, all the mice used in this study are C57BL6/CBA (75%:25%). All animal procedures were performed according to protocols approved by the CNIO-ISCIII Ethics Committe for Research and Animal Welfare (CEIyBA). For additional details, see the Supplemental Experimental Procedures.

Indirect Calorimetry

Indirect calorimetry was performed following standard methods using Oxylet System metabolic chambers (Panlab Harvard Apparatus). To measure the effect of CNIO-PI3Ki on EE, RMR, and VO_2 mice were acclimated for 1 week at 30°C. On the day of analysis, mice were deprived of food and water at 08:00 hr, the compound (15 mg/kg) or its vehicle was administered by gavage at 10:00, and mice were placed in the metabolic chambers. Recordings of VO_2 and VCO_2 from 11:00 to 17:00 were used to calculate EE and RMR. For additional details, see the Supplemental Experimental Procedures.

Measurement of Glucose Uptake by PET

PET analysis was performed following optimized methods previously described by us (Mulero et al., 2011). For additional details, see the Supplemental Experimental Procedures.

Cellular Assays

Isolation and experimentation with MEFs, brown adipocytes, and 3T3-L1 cells were performed using previously established methods. For additional details, see the Supplemental Experimental Procedures.

Reprogramming of MEFs into BAT

In vitro programming of MEFs and subsequent implantation to generate brown adipocytes were performed essentially as previously described (Kajimura et al., 2009). For additional details, see the Supplemental Experimental Procedures.

Measurements of Oxygen Consumption Rate

OCR of brown adipocytes was measured in a Seahorse Bioscience XF24 Extracellular Flux Analyzer (North Billerica, MA, USA). For additional details, see the Supplemental Experimental Procedures.

PI3K Inhibitors

The low molecular weight compound CNIO-PI3Ki is covered by patent WO2010/119264 (files available at the World Intellectual Property Organization, http://www.wipo.int/pctdb/en/wo.jsp?WO=2010119264). This is a potent inhibitor of PI3K isoforms p110α (Ki = 2.4 nM) and p110δ (Ki = 9.8 nM) (inhibition of the other PI3K isoforms, p110β and p110γ, has values of Ki > 100 nM, and inhibition of a total of 282 additional kinases including mTOR and DNAPK requires concentrations of IC_{50} > 1 μM). For in vitro assays, CNIO-PI3Ki was added at a concentration of 1 μM or 10 μM in DMSO, as indicated. For in vivo assays, CNIO-PI3Ki was administered orally by gavage at a dose of 15 mg/kg in 90% PEG-300 and 10% N-methyl-2-pyrrolidone. Treated mice were C57BL6 males, 3 months old. Mice were sacrificed 6 hr later and tissues were extracted and analyzed. The small PI3K inhibitor GDC-0941 was obtained from Shanghai Haoyuan Chemexpress, and LY-294002 was obtained from CalBiochem. Both inhibitors were dissolved DMSO.

SUPPLEMENTAL INFORMATION

Supplemental Information includes seven figures, seven tables, Supplemental Experimental Procedures, and Supplemental References and can be found with this article at doi:10.1016/j.cmet.2012.02.001.

ACKNOWLEDGMENTS

We are grateful to Bruce Spiegelman, Shingo Kajimura, Karl Kaiyala, Carlos Dieguez, and Roger Gomis for advice and reagents. We are also thankful to Cristina Pantoja for help and advice, Gema Iglesias for animal handling, and Javier Martin and Sagrario Ortega for mouse transgenesis. Work in the laboratory of M.S. is funded by the CNIO and by grants from the Spanish Ministry of Science (SAF and CONSOLIDER), the European Research Council (ERC Advanced Grant), and the "Marcelino Botin" Foundation. Work in the laboratory of A.M.V. was funded by grant SAF2009-08114 and by the CIBERDEM (ISCIII), and work in the laboratory of E. Rial was funded by grants SAF2010-20256 and Consolider-Ingenio CSD2007-00020. The funders had no role in study design, data collection and analysis, decision to publish, or preparation of the manuscript. A.O.-M. was recipient of a predoctoral contract of the Regional Government of Madrid. E.L.-G. was recipient of a predoctoral contract from the Spanish Ministry of Education. M.M.G.-B. was supported by the "Ramon y Cajal" program of the Spanish Ministry of Science and Innovation. A.O.-M. performed most of the experiments and contributed to experimental design, data analysis, discussion, and writing of the paper; A.E. contributed to experimental design, data analysis, and discussion; E.L.-G. helped with the experimentation; M.M.-M. performed all the mouse manipulations; G.G.-L. performed the statistical analyses; M.C. performed and diagnosed the histology and pathology; F.M. performed the imaging analyses by DXA and PET; J.P., S.M., and J.R.B. designed, synthesized, and characterized the small molecular weight compound CNIO-PI3Ki; E. Romanos performed indirect calorimetry, activity, and temperature measurements; M.M.G.-B. and E. Rial designed, performed, and interpreted the measurements of respiration; A.M.V. generated the immortalized brown adipocyte lines and provided critical advise; M.S. designed and supervised the study, secured funding, analyzed the data, and wrote the manuscript. All authors discussed the results and commented on the manuscript.

Received: July 6, 2011
Revised: November 16, 2011
Accepted: January 20, 2012
Published online: March 6, 2012

REFERENCES

Arch, J.R., Hislop, D., Wang, S.J., and Speakman, J.R. (2006). Some mathematical and technical issues in the measurement and interpretation of open-circuit indirect calorimetry in small animals. Int. J. Obes. (Lond.) *30*, 1322–1331.

Bartelt, A., Bruns, O.T., Reimer, R., Hohenberg, H., Ittrich, H., Peldschus, K., Kaul, M.G., Tromsdorf, U.I., Weller, H., Waurisch, C., et al. (2011). Brown adipose tissue activity controls triglyceride clearance. Nat. Med. *17*, 200–205.

Bartke, A. (2008). Impact of reduced insulin-like growth factor-1/insulin signaling on aging in mammals: novel findings. Aging Cell *7*, 285–290.

Brand, M.D. (2000). Uncoupling to survive? The role of mitochondrial inefficiency in ageing. Exp. Gerontol. *35*, 811–820.

Butler, A.A., and Kozak, L.P. (2010). A recurring problem with the analysis of energy expenditure in genetic models expressing lean and obese phenotypes. Diabetes *59*, 323–329.

Caldeira da Silva, C.C., Cerqueira, F.M., Barbosa, L.F., Medeiros, M.H., and Kowaltowski, A.J. (2008). Mild mitochondrial uncoupling in mice affects energy metabolism, redox balance and longevity. Aging Cell *7*, 552–560.

Carracedo, A., and Pandolfi, P.P. (2008). The PTEN-PI3K pathway: of feedbacks and cross-talks. Oncogene *27*, 5527–5541.

Chalhoub, N., and Baker, S.J. (2009). PTEN and the PI3-kinase pathway in cancer. Annu. Rev. Pathol. *4*, 127–150.

Chen, Y.F., Wu, C.Y., Kao, C.H., and Tsai, T.F. (2010). Longevity and lifespan control in mammals: lessons from the mouse. Ageing Res. Rev. *9* (*Suppl 1*), S28–S35.

Coschigano, K.T., Holland, A.N., Riders, M.E., List, E.O., Flyvbjerg, A., and Kopchick, J.J. (2003). Deletion, but not antagonism, of the mouse growth hormone receptor results in severely decreased body weights, insulin, and

insulin-like growth factor I levels and increased life span. Endocrinology *144*, 3799–3810.

Cypess, A.M., Lehman, S., Williams, G., Tal, I., Rodman, D., Goldfine, A.B., Kuo, F.C., Palmer, E.L., Tseng, Y.H., Doria, A., et al. (2009). Identification and importance of brown adipose tissue in adult humans. N. Engl. J. Med. *360*, 1509–1517.

Di Cristofano, A., Pesce, B., Cordon-Cardo, C., and Pandolfi, P.P. (1998). Pten is essential for embryonic development and tumour suppression. Nat. Genet. *19*, 348–355.

Dorman, J.B., Albinder, B., Shroyer, T., and Kenyon, C. (1995). The age-1 and daf-2 genes function in a common pathway to control the lifespan of Caenorhabditis elegans. Genetics *141*, 1399–1406.

Dranka, B.P., Benavides, G.A., Diers, A.R., Giordano, S., Zelickson, B.R., Reily, C., Zou, L., Chatham, J.C., Hill, B.G., Zhang, J., et al. (2011). Assessing bioenergetic function in response to oxidative stress by metabolic profiling. Free Radic. Biol. Med. *51*, 1621–1635.

Feige, J.N., Lagouge, M., Canto, C., Strehle, A., Houten, S.M., Milne, J.C., Lambert, P.D., Mataki, C., Elliott, P.J., and Auwerx, J. (2008). Specific SIRT1 activation mimics low energy levels and protects against diet-induced metabolic disorders by enhancing fat oxidation. Cell Metab. *8*, 347–358.

Fontana, L., Partridge, L., and Longo, V.D. (2010). Extending healthy life span—from yeast to humans. Science *328*, 321–326.

Gates, A.C., Bernal-Mizrachi, C., Chinault, S.L., Feng, C., Schneider, J.G., Coleman, T., Malone, J.P., Townsend, R.R., Chakravarthy, M.V., and Semenkovich, C.F. (2007). Respiratory uncoupling in skeletal muscle delays death and diminishes age-related disease. Cell Metab. *6*, 497–505.

Guerra, C., Navarro, P., Valverde, A.M., Arribas, M., Bruning, J., Kozak, L.P., Kahn, C.R., and Benito, M. (2001). Brown adipose tissue-specific insulin receptor knockout shows diabetic phenotype without insulin resistance. J. Clin. Invest. *108*, 1205–1213.

Hempenstall, S., Picchio, L., Mitchell, S.E., Speakman, J.R., and Selman, C. (2010). The impact of acute caloric restriction on the metabolic phenotype in male C57BL/6 and DBA/2 mice. Mech. Ageing Dev. *131*, 111–118.

Jiang, W., Zhu, Z., and Thompson, H.J. (2008). Dietary energy restriction modulates the activity of AMP-activated protein kinase, Akt, and mammalian target of rapamycin in mammary carcinomas, mammary gland, and liver. Cancer Res. *68*, 5492–5499.

Kaiyala, K.J., and Schwartz, M.W. (2011). Toward a more complete (and less controversial) understanding of energy expenditure and its role in obesity pathogenesis. Diabetes *60*, 17–23.

Kajimura, S., Seale, P., Kubota, K., Lunsford, E., Frangioni, J.V., Gygi, S.P., and Spiegelman, B.M. (2009). Initiation of myoblast to brown fat switch by a PRDM16-C/EBP-beta transcriptional complex. Nature *460*, 1154–1158.

Kamagate, A., Kim, D.H., Zhang, T., Slusher, S., Gramignoli, R., Strom, S.C., Bertera, S., Ringquist, S., and Dong, H.H. (2010). Forkhead box O1 links hepatic insulin action to endoplasmic reticulum stress. Endocrinology *151*, 3521–3535.

Karamanlidis, G., Karamitri, A., Docherty, K., Hazlerigg, D.G., and Lomax, M.A. (2007). C/EBPbeta reprograms white 3T3-L1 preadipocytes to a Brown adipocyte pattern of gene expression. J. Biol. Chem. *282*, 24660–24669.

Kenyon, C.J. (2010). The genetics of ageing. Nature *464*, 504–512.

Kops, G.J., de Ruiter, N.D., De Vries-Smits, A.M., Powell, D.R., Bos, J.L., and Burgering, B.M. (1999). Direct control of the Forkhead transcription factor AFX by protein kinase B. Nature *398*, 630–634.

Kozak, L.P., and Anunciado-Koza, R. (2008). UCP1: its involvement and utility in obesity. Int. J. Obes. (Lond.) *32* (*Suppl 7*), S32–S38.

Li, B., Nolte, L.A., Ju, J.S., Han, D.H., Coleman, T., Holloszy, J.O., and Semenkovich, C.F. (2000). Skeletal muscle respiratory uncoupling prevents diet-induced obesity and insulin resistance in mice. Nat. Med. *6*, 1115–1120.

Li, X., Monks, B., Ge, Q., and Birnbaum, M.J. (2007). Akt/PKB regulates hepatic metabolism by directly inhibiting PGC-1alpha transcription coactivator. Nature *447*, 1012–1016.

Lidell, M.E., and Enerback, S. (2010). Brown adipose tissue–a new role in humans? Nat. Rev. Endocrinol. *6*, 319–325.

Lin, J., Wu, H., Tarr, P.T., Zhang, C.Y., Wu, Z., Boss, O., Michael, L.F., Puigserver, P., Isotani, E., Olson, E.N., et al. (2002). Transcriptional co-activator PGC-1 alpha drives the formation of slow-twitch muscle fibres. Nature *418*, 797–801.

Masse, I., Molin, L., Billaud, M., and Solari, F. (2005). Lifespan and dauer regulation by tissue-specific activities of Caenorhabditis elegans DAF-18. Dev. Biol. *286*, 91–101.

Matheu, A., Maraver, A., Klatt, P., Flores, I., Garcia-Cao, I., Borras, C., Flores, J.M., Vina, J., Blasco, M.A., and Serrano, M. (2007). Delayed ageing through damage protection by the Arf/p53 pathway. Nature *448*, 375–379.

Matheu, A., Maraver, A., Collado, M., Garcia-Cao, I., Canamero, M., Borras, C., Flores, J.M., Klatt, P., Vina, J., and Serrano, M. (2009). Anti-aging activity of the Ink4/Arf locus. Aging Cell *8*, 152–161.

Matsumoto, M., Han, S., Kitamura, T., and Accili, D. (2006). Dual role of transcription factor FoxO1 in controlling hepatic insulin sensitivity and lipid metabolism. J. Clin. Invest. *116*, 2464–2472.

Matsumoto, M., Pocai, A., Rossetti, L., Depinho, R.A., and Accili, D. (2007). Impaired regulation of hepatic glucose production in mice lacking the forkhead transcription factor Foxo1 in liver. Cell Metab. *6*, 208–216.

Miller, R.A., Harper, J.M., Galecki, A., and Burke, D.T. (2002). Big mice die young: early life body weight predicts longevity in genetically heterogeneous mice. Aging Cell *1*, 22–29.

Mookerjee, S.A., Divakaruni, A.S., Jastroch, M., and Brand, M.D. (2011). Mitochondrial uncoupling and lifespan. Mech. Ageing Dev. *131*, 463–472.

Moore, T., Beltran, L., Carbajal, S., Strom, S., Traag, J., Hursting, S.D., and DiGiovanni, J. (2008). Dietary energy balance modulates signaling through the Akt/mammalian target of rapamycin pathways in multiple epithelial tissues. Cancer Prev. Res. (Phila. Pa.) *1*, 65–76.

Morris, J.Z., Tissenbaum, H.A., and Ruvkun, G. (1996). A phosphatidylinositol-3-OH kinase family member regulating longevity and diapause in Caenorhabditis elegans. Nature *382*, 536–539.

Mulero, F., Donate, L.E., and Serrano, M. (2011). Imaging cancer in mice by PET, CT, and combined PET-CT. Curr. Protoc. Mouse Biol. *1*, 85–103.

Nakamura, N., Ramaswamy, S., Vazquez, F., Signoretti, S., Loda, M., and Sellers, W.R. (2000). Forkhead transcription factors are critical effectors of cell death and cell cycle arrest downstream of PTEN. Mol. Cell. Biol. *20*, 8969–8982.

Nedergaard, J., and Cannon, B. (2010). The changed metabolic world with human brown adipose tissue: therapeutic visions. Cell Metab. *11*, 268–272.

Nedergaard, J., Bengtsson, T., and Cannon, B. (2011). New powers of brown fat: fighting the metabolic syndrome. Cell Metab. *13*, 238–240.

Nicholls, D.G., and Locke, R.M. (1984). Thermogenic mechanisms in brown fat. Physiol. Rev. *64*, 1–64.

Pfluger, P.T., Herranz, D., Velasco-Miguel, S., Serrano, M., and Tschop, M.H. (2008). Sirt1 protects against high-fat diet-induced metabolic damage. Proc. Natl. Acad. Sci. USA *105*, 9793–9798.

Podsypanina, K., Ellenson, L.H., Nemes, A., Gu, J., Tamura, M., Yamada, K.M., Cordon-Cardo, C., Catoretti, G., Fisher, P.E., and Parsons, R. (1999). Mutation of Pten/Mmac1 in mice causes neoplasia in multiple organ systems. Proc. Natl. Acad. Sci. USA *96*, 1563–1568.

Puig, O., and Tjian, R. (2005). Transcriptional feedback control of insulin receptor by dFOXO/FOXO1. Genes Dev. *19*, 2435–2446.

Puigserver, P., and Spiegelman, B.M. (2003). Peroxisome proliferator-activated receptor-gamma coactivator 1 alpha (PGC-1 alpha): transcriptional coactivator and metabolic regulator. Endocr. Rev. *24*, 78–90.

Puigserver, P., Wu, Z., Park, C.W., Graves, R., Wright, M., and Spiegelman, B.M. (1998). A cold-inducible coactivator of nuclear receptors linked to adaptive thermogenesis. Cell *92*, 829–839.

Puigserver, P., Rhee, J., Donovan, J., Walkey, C.J., Yoon, J.C., Oriente, F., Kitamura, Y., Altomonte, J., Dong, H., Accili, D., et al. (2003). Insulin-regulated hepatic gluconeogenesis through FOXO1-PGC-1alpha interaction. Nature *423*, 550–555.

Renner, O., and Carnero, A. (2009). Mouse models to decipher the PI3K signaling network in human cancer. Curr. Mol. Med. *9*, 612–625.

Seale, P., Kajimura, S., Yang, W., Chin, S., Rohas, L.M., Uldry, M., Tavernier, G., Langin, D., and Spiegelman, B.M. (2007). Transcriptional control of brown fat determination by PRDM16. Cell Metab. *6*, 38–54.

Selman, C., and Withers, D.J. (2011). Mammalian models of extended healthy lifespan. Philos. Trans. R. Soc. Lond. B Biol. Sci. *366*, 99–107.

Serrano, M., and Blasco, M.A. (2007). Cancer and ageing: convergent and divergent mechanisms. Nat. Rev. Mol. Cell Biol. *8*, 715–722.

Song, M.S., Carracedo, A., Salmena, L., Song, S.J., Egia, A., Malumbres, M., and Pandolfi, P.P. (2011). Nuclear PTEN regulates the APC-CDH1 tumor-suppressive complex in a phosphatase-independent manner. Cell *144*, 187–199.

Speakman, J.R., Talbot, D.A., Selman, C., Snart, S., McLaren, J.S., Redman, P., Krol, E., Jackson, D.M., Johnson, M.S., and Brand, M.D. (2004). Uncoupled and surviving: individual mice with high metabolism have greater mitochondrial uncoupling and live longer. Aging Cell *3*, 87–95.

Stambolic, V., Tsao, M.S., Macpherson, D., Suzuki, A., Chapman, W.B., and Mak, T.W. (2000). High incidence of breast and endometrial neoplasia resembling human Cowden syndrome in pten+/− mice. Cancer Res. *60*, 3605–3611.

Suzuki, A., de la Pompa, J.L., Stambolic, V., Elia, A.J., Sasaki, T., del Barco Barrantes, I., Ho, A., Wakeham, A., Itie, A., Khoo, W., et al. (1998). High cancer susceptibility and embryonic lethality associated with mutation of the PTEN tumor suppressor gene in mice. Curr. Biol. *8*, 1169–1178.

Um, S.H., Frigerio, F., Watanabe, M., Picard, F., Joaquin, M., Sticker, M., Fumagalli, S., Allegrini, P.R., Kozma, S.C., Auwerx, J., et al. (2004). Absence of S6K1 protects against age- and diet-induced obesity while enhancing insulin sensitivity. Nature *431*, 200–205.

Um, S.H., D'Alessio, D., and Thomas, G. (2006). Nutrient overload, insulin resistance, and ribosomal protein S6 kinase 1, S6K1. Cell Metab. *3*, 393–402.

Utermark, T., Schaffhausen, B.S., Roberts, T.M., and Zhao, J.J. (2007). The p110alpha isoform of phosphatidylinositol 3-kinase is essential for polyomavirus middle T antigen-mediated transformation. J. Virol. *81*, 7069–7076.

van der Horst, A., and Burgering, B.M. (2007). Stressing the role of FoxO proteins in lifespan and disease. Nat. Rev. Mol. Cell Biol. *8*, 440–450.

van Marken Lichtenbelt, W.D., Vanhommerig, J.W., Smulders, N.M., Drossaerts, J.M., Kemerink, G.J., Bouvy, N.D., Schrauwen, P., and Teule, G.J. (2009). Cold-activated brown adipose tissue in healthy men. N. Engl. J. Med. *360*, 1500–1508.

Vega, R.B., Huss, J.M., and Kelly, D.P. (2000). The coactivator PGC-1 cooperates with peroxisome proliferator-activated receptor alpha in transcriptional control of nuclear genes encoding mitochondrial fatty acid oxidation enzymes. Mol. Cell. Biol. *20*, 1868–1876.

Virtanen, K.A., Lidell, M.E., Orava, J., Heglind, M., Westergren, R., Niemi, T., Taittonen, M., Laine, J., Savisto, N.J., Enerback, S., et al. (2009). Functional brown adipose tissue in healthy adults. N. Engl. J. Med. *360*, 1518–1525.

Wang, C., Jurk, D., Maddick, M., Nelson, G., Martin-Ruiz, C., and von Zglinicki, T. (2009). DNA damage response and cellular senescence in tissues of aging mice. Aging Cell *8*, 311–323.

Zhou, Y., Xu, B.C., Maheshwari, H.G., He, L., Reed, M., Lozykowski, M., Okada, S., Cataldo, L., Coschigamo, K., Wagner, T.E., et al. (1997). A mammalian model for Laron syndrome produced by targeted disruption of the mouse growth hormone receptor/binding protein gene (the Laron mouse). Proc. Natl. Acad. Sci. USA *94*, 13215–13220.

Zhao, J.J., Cheng, H., Jia, S., Wang, L., Gjoerup, O.V., Mikami, A., and Roberts, T.M. (2006). The p110alpha isoform of PI3K is essential for proper growth factor signaling and oncogenic transformation. Proc. Natl. Acad. Sci. USA *103*, 16296–16300.